Food Hydrocolloids 90 (2019) 9–18

Contents lists available at ScienceDirect

Food Hydrocolloids

journal homepage: www.elsevier.com/locate/foodhyd

Rheological properties and structure modification in liquid and gel of tilapia skin gelatin by the addition of low acyl gellan

Li Cheng Sow[a,b], Si Jia Tan[a], Hongshun Yang[a,b,*]

[a] Food Science and Technology Programme, C/o Department of Chemistry, National University of Singapore, 3 Science Drive 3, Singapore, 117543, Singapore
[b] National University of Singapore (Suzhou) Research Institute, 377 Lin Quan Street, Suzhou Industrial Park, Suzhou, Jiangsu, 215123, PR China

ARTICLE INFO

Keywords:
Fish gelatin
Confocal laser scanning microscopy
Rheology
Microstructure
Texture
Polysaccharide

ABSTRACT

Fish gelatin (FG) was modified by low acyl gellan (Ge) to produce a replacer for pork gelatin (PG). Increasing mixing ratio of Ge:FG (w/w) modified rheological properties and structure of FG progressively. The largest of FG-Ge complex coacervates (1775 ± 593 nm) formed at Ge:FG (w/w) of 7.5:92.5, driven by electrostatic interaction between FG and Ge. However, the network density was reduced by the formation of large complex coacervates (fractal dimension, d_f 2.45 ± 0.01 in FG-Ge vs. 2.48 ± 0.00 in FG). The non-interacting FG re-associated to a greater extent into triple helix (helix/coil ratio, 3.10 ± 0.93 in FG-Ge vs. 0.58 ± 0.07 in FG), therefore increased the rigidity of the gel. The mixed gel was stronger and more stable, with lower compliances (J_0, J_{m1}) and a higher melting temperature (T_m) than FG. The mixed gel at a Ge:FG (w/w) of 1:99 had similar rheological properties to PG. A schematic model was proposed to illustrate the progressive modification of FG by Ge.

1. Introduction

Fish gelatin (FG) is a potential mammalian gelatin replacer that is more religiously acceptable than beef gelatin (BG) or pork gelatin (PG) (Feng, Bansal, & Yang, 2016; Feng, Fu, & Yang, 2017; Feng, Ng, Mikš-Krajnik, & Yang, 2017). Muslims will account for 29.7% of the world's population by 2050 (Desilver & Masci, 2017); however, the current gelatin market is dominated (> 98%) by PG and BG (Sow et al., 2017). One of the major limitations of FG compared with mammalian gelatin is the difference in rheological properties (Mohtar, Perera, Quek, & Hemar, 2013; Pang, Deeth, Yang, Prakash, & Bansal, 2017). The proline and hydroxyproline contents in tilapia FG are about 11% lower than pork gelatin (Zhou, Mulvaney, & Regenstein, 2006), thus the gel has lower strength, gelling and melting temperature (T_g and T_m, respectively) (Haug, Draget, & Smidsrød, 2004).

Gellan is produced by *Sphingomonas elodea*, and the structure of deacylated gellan consists of repeating tetrasaccharide with one negatively charged COO^- group on glucuronic acid (Morris, Nishinari, & Rinaudo, 2012). Gelation of gellan involves the formation of a double helix and the subsequent aggregation of the double helices, which is ion sensitive (Hu, Lu, Zhao, & Matsukawa, 2017).

Mixing of low acyl gellan (Ge) and gelatin has been explored, and combinations of gelling agents could provide desirable textures or perform protein-polysaccharide interactions (Banerjee & Bhattacharya, 2011). Papageorgiou, Kasapis, and Richardson (1994) reported synergistic enhancement of the physical properties of a binary gel of Ge-PG, with the continuous phase transition from Ge into PG when the PG:Ge > 5.0:0.5. Lau, Tang, and Paulson (2000, 2001) mixed Ge (1.6–2%, w/v) and BG (0–1.4%, w/v) and $CaCl_2$ (0–30 mM), and observed that the hardness, gelation rate, T_g, and turbidity increased with increasing Ge. Lee et al. (2003); Lee, Shim, and Lee (2004) mixed PG (0.2–1.6%, w/v) and Ge (2–0.2%, w/v), and noted that the gel with 0.4% PG and 0.6% Ge had the maximum hardness. Ikeda and Henry (2016) suggested that 6.025% (w/w) type A gelatin and 0.075% (w/w) Ge could mimic the texture characteristic of 7.1% (w/w) gelatin gummy confection.

As for the effect of mixing FG and Ge, Pranoto, Lee, and Park (2007) prepared a film of Ge-FG (2 g Ge/100 g FG) with improved T_m, and tensile strength. Previously, we reported that mixtures of 6.67% (w/v) FG-0.1% (w/v) Ge and 20 mM $CaCl_2$ or 5.925% FG-0.025% Ge and 3 mM $CaCl_2$ mimicked the T_m and texture of 6.67% (w/v) BG and 6% (w/v) PG, respectively (Sow et al., 2017; Sow, Kong, & Yang, 2018b). Similarly, Petcharat and Benjakul (2017) reported mixing of Ge and FG to improve gel strength, hardness, T_m, and T_g without an adverse sensory effect at 0.167% of Ge in a 6.67% (w/v) gel.

The aim of the current research was to characterise the rheological

* Corresponding author. Food Science and Technology Programme, c/o Department of Chemistry, National University of Singapore, 3 Science Drive 3, Singapore, 117543, Singapore.
E-mail address: chmynghs@nus.edu.sg (H. Yang).

https://doi.org/10.1016/j.foodhyd.2018.12.006
Received 2 August 2018; Received in revised form 29 November 2018; Accepted 4 December 2018
Available online 05 December 2018
0268-005X/

properties of Ge-FG blends in terms of the gelling mechanism, mechanical strength, and stability of the gel under different temperature, frequencies and shear stresses. The application of a Ge-FG blend as a mammalian gelatin replacer cannot be confirmed without the rheological characterisation. In contrast to previous studies in which Ge was used as a major component of the blend (Lau et al., 2000; Lee et al., 2003), the ratio of Ge:FG in this study was capped at 20:80, to avoid over modification of FG. The Winter-Chambon scaling law was applied for the first time to investigate the gelling mechanism of Ge-FG gels (Yang, Yang, & Yang, 2018b), while Burgers model coupled with a creep-recovery test quantified the response of the gels to constant stress (Sow, Chong, Liao, & Yang, 2018a). Together with the interaction and structural analysis, a complete picture of Ge as mammalian gelatin replacer was obtained.

2. Materials and methods

2.1. Materials

PG (240 Bloom) was purchased from Chengdu Classic Gelatin Co. Ltd (Chengdu, Sichuan, China) and the tilapia skin gelatin (FG) (180 Bloom) was purchased from Jiangxi Cosen Biology Co., Ltd (Yingtan, Jiangxi, China). Low acyl gellan (Ge) was supplied from FMC Health and Nutrition (Philadelphia, PA, USA). The ion contents (Na, Ca, and K) and the viscosity-averaged molecular weight ($\overline{M_v}$) was previously analysed and reported in Sow et al. (2018b). Rhodamine B, fluorescein isothiocyanate (FITC), and dimethyl sulphoxide (DMSO) were obtained from Merck KGaA (Darmstadt, Germany).

2.2. Sample preparation

A series of FG-Ge mixtures and the control samples of FG, PG, and Ge in both liquid (0.5%, w/v) and gel (6.67%, w/v; 2% (w/v) for Ge) forms were prepared according to Table 1. The preparation procedure was described in Sow et al. (2018a) with slight modification. Briefly, dried FG was soaked in deionised (DI) water for 2 h and heated to 65 °C until dissolved, while Ge was separately heated and stirred in 90 °C DI water until dissolved. The solutions were then mixed for 30 min at 85 °C according to the Ge:FG (w/w) ratios shown in Table 1. The samples had a pH of about 6.01–6.22, which was below the isoelectric point (pI) of FG (pH 7.52).

2.3. Turbidity

Liquid samples (0.5%, w/v) were cooled from 85 to 25 °C. Measurement of absorbance at 600 nm was performed using a UV-1700 spectrophotometer (Shimadzu Corporation, Kyoto, Japan), turbidity (τ) was reported according to the following equation,

$$\tau = -\left(\frac{1}{L}\right)\ln\left(\frac{I}{I_0}\right) \quad (1)$$

where L is the length of the optical path (cm), I is the transmitted radiation intensity, and I_0 is the incident radiation intensity (Sow et al., 2017).

Table 1
Formulation of fish gelatin (FG) and gellan (Ge) mixtures (FGe) used in the experiments.

Sample	Mixing ratio (w/w)		Actual concentration at 0.5% (%, w/v)		Actual concentration at 6.67% (%, w/v)	
	FG	Ge	FG	Ge	FG	Ge
FG	100.00	0.00	0.50000	0.00000	6.670	0.000
FGe1	99.75	0.25	0.49875	0.00125	–	–
FGe2	99.50	0.50	0.49750	0.00250	6.630	0.033
FGe3	99.25	0.75	0.49625	0.00375	–	–
FGe4	99.00	1.00	0.49500	0.00500	6.600	0.067
FGe5	97.50	2.50	0.48750	0.01250	6.500	0.167
FGe6	95.00	5.00	0.47500	0.02500	–	–
FGe7	92.50	7.50	0.46250	0.03750	6.167	0.500
FGe8	90.00	10.00	0.45000	0.05000	–	–
FGe9	80.00	20.00	0.40000	0.10000	5.333	1.333
Ge	0.00	100.00	0.00000	0.50000	0.000	2.000[#]

[#]Ge was prepared at 2% (w/v) instead of 6.67% (w/v), as it is difficult to dissolve a high concentration of gellan.

2.4. Particle size and zeta potential

To ensure the samples were within the count rate limit, liquid samples (0.5%, w/v) were diluted with hot DI water to 0.01% (w/v) before cooling to 25 °C. A NanoBrook Omni Particle Size and Zeta Potential analyzer (Brookhaven Instruments, NY, USA) was used to perform dynamic light scattering (DLS) and phase analysis light scattering to determine the particle size and zeta potential, respectively (Sow et al., 2017).

2.5. Confocal laser scanning microscopy (CLSM)

Rhodamine B was selected to label FG and FITC was used to label Ge as described in Sow et al. (2018b) and Feng, Hang, Zhou, Liu, and Yang (2018). FG and Ge stock solutions were prepared and adjusted to pH 10.5 and 8.5, respectively. Fluorescent dye (25 μL) in DMSO (2%, w/v) was added to 100 mL of stock solution and stirred for 90 min at 85 °C, and re-adjusted to the original pH before mixing of FG and Ge. A cover glass slide (0.13–0.16 mm thickness) was used for liquid (0.5%, w/v) (20 μL), while a cuvette with thin glass bottom was used to contain the gel (6.67%, w/v) (0.3 mL). The samples were stored under lightproof conditions overnight at 4 ± 2 °C, then analysed by an Olympus confocal scanning unit (Fluoview FV 1000, Tokyo, Japan) equipped argon ion and Helium−Neon (HeNe) lasers. The images captured were at 60× magnification (PlanApo 60×/1.0 WLSM 0.17) with water immersion. Fluoview software (Olympus, Tokyo, Japan) was used for the image processing.

2.6. Rheological tests

A controlled-stress rheometer (MCR102, Anton Paar, Graz, Austria) was used for rheological characterisation of the gels. Hot solutions were poured onto the rheometer and covered with a thin layer of corn coil (Yang, Yang, & Yang, 2018a). The samples were pre-sheared at 85 °C for 10 min (1% strain, 1 rad/s angular frequency, ω), before four testing protocols were applied. A 25-mm diameter stainless-steel parallel plate was used for protocols 1 and 2, and a 60-mm diameter stainless-steel cone plate (angle: 1°, 0.1667 mm gap) was used for protocols 3 and 4. Protocol 1: the sample was cooled from 85 to 10 °C at a rate of 1 °C/min (1% strain, 1 rad/s); the gel formed was then heated from 10 to 85 °C. The T_m and T_g were determined as the temperature when storage modulus (G′) and loss modulus (G″) crossed over (Sow et al., 2018b). Protocol 2: to determine the critical gelation temperature (T_g*), frequency sweeps (100–1 rad/s, 1% strain) were carried out at temperatures near the T_g. According to the Winter-Chambon equation (Winter & Chambon, 1986), at the critical gelling point,

$$G'(\omega) \sim G''(\omega) \sim \omega^n. \quad (2)$$

$$\tan\ \delta = \frac{G''(\omega)}{G'(\omega)} = \tan\frac{n\pi}{2}. \quad (3)$$

where n is the critical relaxation component, and tan δ is the loss factor.

The power law behaviour at the critical gelling point could also be expressed as,

$$G(t) = S_g t^{-n}. \quad (4)$$

$$G'(\omega) = G''(\omega)/\tan\frac{n\pi}{2} = S_g\omega^n\Gamma(1-n)\cos\frac{n\pi}{2}. \quad (5)$$

where $G(t)$ is the relaxation modulus, S_g is the critical gel strength, $\Gamma(1-n)$ is the Gamma function, G′ or G″ at the critical gelling point and n would be used to calculate S_g using Eq. (5) (Yang et al., 2018a).

Protocol 3: the sample was cooled from 85 to 10 °C at 1 °C/min, a time sweep was conducted for 90 min at 10 °C (1% strain, 1 rad/s). A frequency sweep from 0.1 to 100 rad/s (1% strain, 10 °C) was carried out. The complex viscosity, η* and ω showed a power law relationship (Nakauma et al., 2016),

$$\eta^*(\omega) = K_f\omega^{-n_f} \quad (0 < n_f < 1). \quad (6)$$

$$\eta^* = \frac{\sqrt{(G')^2 + (G'')^2}}{\omega}. \quad (7)$$

where K_f is the dynamic consistency index, and n_f is the dynamic power law factor.

Protocol 4: finally, the gel was subject to creep-recovery test. A constant shear stress of 200 Pa was applied from 0 to 915.5 s (creep-phase). After that, the gel was allowed to recover from 915.5 to 1820 s at 0 Pa (recovery phase). Burgers model was applied to describe the changes in compliance, J(t) over time (Sow et al., 2018a).

$$J(t) = \gamma/\sigma, \quad (8)$$

where γ is the shear strain and σ is the shear stress of the creep phase.

During the creep phase,

$$J(t)_c = J_{0_c} + \sum_{i=1}^{3}\left[J_{m_{i_c}}\left(1 - e^{\frac{-t}{\lambda_{i_c}}}\right)\right] + \frac{t}{\eta_0}. \quad (9)$$

While during recovery phase,

$$J(t)_r = J_{max} - J_{0_r} - \sum_{i=1}^{3}\left[J_{m_{i_r}}\left(1 - e^{\frac{-t}{\lambda_{i_r}}}\right)\right]. \quad (10)$$

where J_0, J_m, and J_{max} are defined as instantaneous, viscoelastic, and maximum compliance, respectively, t and λ are the time and retardation time, respectively, and η_0 is the zero-shear viscosity.

2.7. Fourier transform infrared (FTIR) spectroscopy

Lyophilised gel (6.67%, w/v) was milled into a powder and homogenised with KBr (3 mg sample/100 mg KBr) for pellet formation. The FTIR spectra (4000–500 cm^{-1}) were recorded with 64 scans and a resolution of 4 cm^{-1}, using a Spectrum One FTIR spectrometer (PerkinElmer, Waltham, MA, USA) (Sow & Yang, 2015). Before every scan, background spectra were recorded and corrected. The spectra were baseline-corrected, smoothed, and normalised using Spectrum software. Amide I (1600–1700 cm^{-1}) was deconvoluted and curve-fitted using Origin Pro 9 (OriginLab, Northampton, MA, USA).

2.8. Statistical analysis

Triplicate independent experiments with at least duplicate measurements within each run were conducted. The results are reported as the mean ± standard deviation. One-way analysis of variance (ANOVA) and Duncan's multiple range test were performed using SPSS Statistics 20 software (IBM, Chicago, IL, USA) to determine statistical differences ($P < 0.05$) within and between test groups.

3. Results and discussions

3.1. Turbidity, particle size, and zeta potential

When two biopolymers are mixed together, associative or segregative interactions occur (Morris et al., 2012). In Fig. 1A, increased

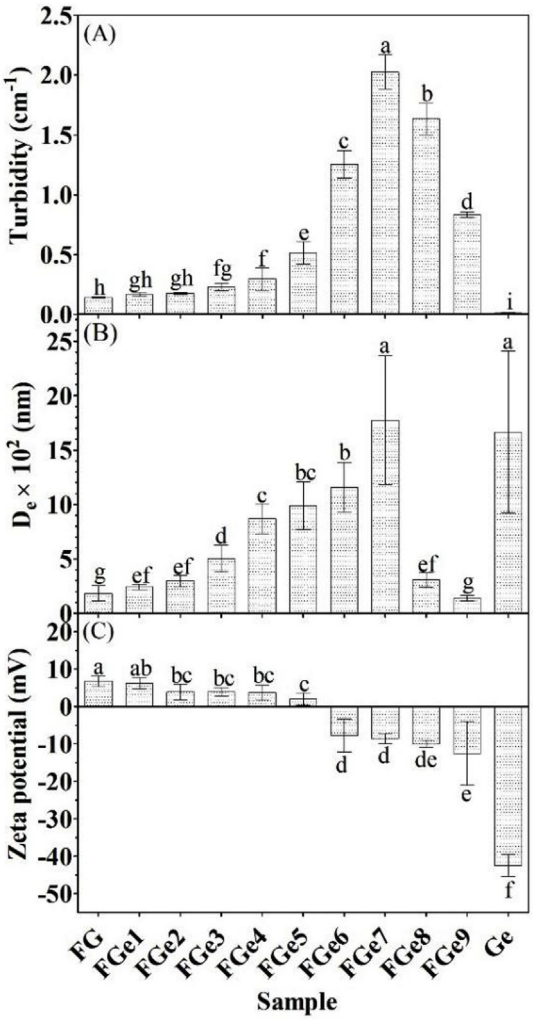

Fig. 1. Effect of the mixing of gellan (Ge) with fish gelatin (FG) on (A) turbidity, (B) effective diameter (D_{50}), and (C) zeta potential of the mixtures (0.5%, w/v).
*Means with different lowercase letters are significantly different ($P < 0.05$) among different groups.
*FGe2, FGe4, FGe5, FGe7, and FGe9 refer to FG-Ge mixtures with mixing ratios (Ge:FG, w/w) of 0.5:99.5, 1:99, 2.5:97.5, 7.5:92.5, and 20:80, respectively.

turbidity of FG-Ge mixtures was observed from FGe1 to FGe7. Both FG and Ge have turbidities lower than the mixtures, thus the increase in turbidity is likely to arise from associative phase separation (Banerjee & Bhattacharya, 2011). FG carries a positive charge (6.7 ± 1.5 mV) while Ge carries a negative charge (−42.5 ± 2.9 mV); therefore, an electrostatic interaction could drive the formation of complex coacervates of FG-Ge. The formation of complex coacervates led to an increase in the effective diameter, D_e (Fig. 1B): the D_e increased from 183 ± 70 nm in FG to 1775 ± 594 nm in FGe7. Ge had a large D_e (1664 ± 744 nm), which was attributed to the intramolecular aggregation of Ge (0.01%, w/v) below the gelling concentration (≥0.167%, w/v, Fig. S1) (Morris et al., 2012). In contrast, at a higher concentration (0.5%, w/v) the turbidity of Ge remained low because of the formation of soft fluid gel network rather than aggregates.

In the mixture of FG-κ-carrageenan (KC), the maximum turbidity and D_e of FG-KC occurred simultaneously when the zeta potential switched from positive to negative, a sign of neutralisation of the surface charge caused by electrostatic interaction (Sow et al., 2018a). This was not the case for the FG-Ge sample, the zeta potential approached to neutral at FGe5 (2.0 ± 1.6 mV), while the D_e and turbidity increased continuously to a maximum at FGe7 (−8.6 ± 1.4 mV). This might indicate that other interactions, such as hydrogen bonds, could lead to

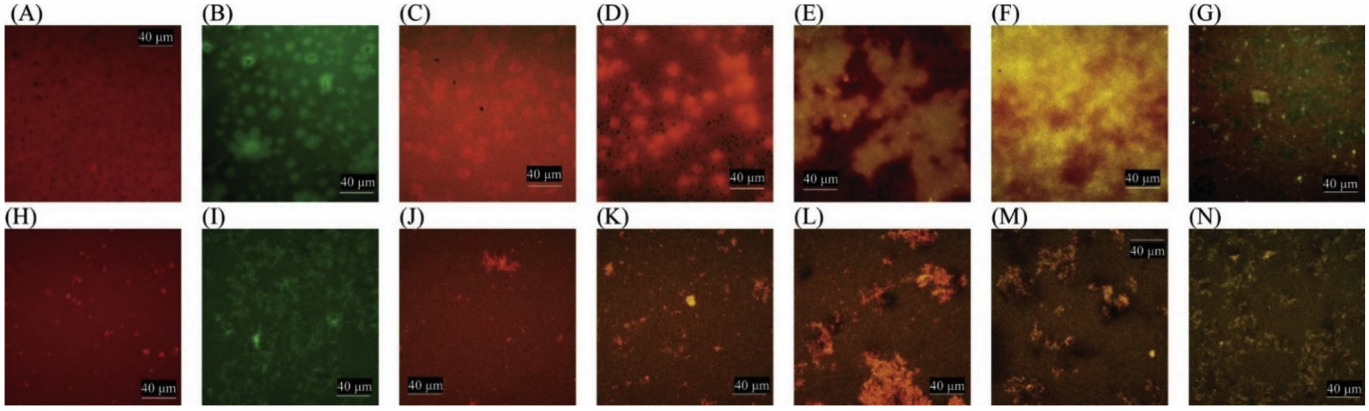

Fig. 2. Microstructure of (A–G) solution (0.5%, w/v) and (H–N) gel (6.67%, w/v) of (A, H) fish gelatin (FG), (B, I) gellan (Ge), and the FG-Ge mixtures (FGe), including (C, J) FGe2, (D, K) FGe4, (E, L) FGe5, (F, M) FGe7, and (G, N) FGe9.
*FGe2, FGe4, FGe5, FGe7, and FGe9 refer to FG-Ge mixtures with mixing ratios (Ge:FG, w/w) of 0.5:99.5, 1:99, 2.5:97.5, 7.5:92.5, and 20:80, respectively.

progressive aggregation of FG-Ge complex coacervates. Alternatively, the growth in turbidity and D_e might be the result of segregative FG-Ge interaction, because the D_e of FGe7 was similar to that of Ge. Excess Ge that was not bound to FG would form aggregates, increasing the turbidity and D_e. The segregative interaction became prominent in FGe8 and FGe9. Segregative interaction resulted in steric exclusion between FG and Ge, which increased the effective concentration of the two biopolymers and formed a bi-continuous structure (Papageorgiou et al., 1994). The decreased in D_e of FGe8 and FGe9 (Fig. 1B) indicated little or no formation of complex coacervates.

3.2. CLSM

The microstructure of FG, Ge, and the mixtures were captured in solution (0.5%, w/v) and as gels (6.67%, w/v) (Fig. 2). Spherical aggregates of FG (Fig. 2A, H) and irregular, fibrous like aggregates of Ge (Fig. 2B, I) were found. The fibrous-like structure of Ge was consistent with the observation of Sow et al. (2018b) under atomic force microscopy. In liquid, small spherical FG-Ge complex coacervates were found in FGe2 and FGe4 (Fig. 2C and D), similar to those observed by Chilvers and Morris (1987). The aggregates joined together into large irregular complexes in FGe5 and FGe7 (Fig. 2E and F), and almost completely disappeared in FGe9 (Fig. 2G, N). Wang and Padua (2010) found that microsphere of zein could aggregate, merge and fuse in one phase under tight packing when concentration increased. The yellow aggregates indicated that both FG (red) and Ge (green) participated in the formation of complex coacervates. In FGe9, separate FG and Ge regions showed a bi-continuous structure. It was proposed that the high turbidity and large D_e of FGe7 might be caused by the association of complex coacervates or the segregation of Ge aggregates. From Fig. 2D, the former argument was supported by the aggregation of complex coacervates into cloud-like aggregates.

Comparing between liquid and gel states, we found that the size of FG aggregates increased when concentration increased from 0.5% (Fig. 2A) to 6.67% (w/v) (Fig. 2H). While for Ge, the structure changed from irregular and spherical-like aggregates in liquid state (Fig. 2B) to fibrous-like aggregates in gel state (Fig. 2I). The coarse holes that appeared in liquid state (Fig. 2A and B) disappeared when in gel state, indicating that the gel had a denser structure than liquid. The microstructure of large voids and strands could be related to the decreased resistance of gel external force (Sinthusamran, Benjakul, & Kishimura, 2014). The addition of Ge modified the gel microstructure by altering the distribution of the holes, thus the FGe2 (Fig. 2C, J) had a dense and homogenous structure, while there were increasing number and size of holes in FGe4, FGe5, and FGe7 (Fig. 2D–F, K-M).

Although FG is the dominant biopolymer based on the Ge:FG (w/w) of 20:80 in FGe9, Ge formed the continuous phase (green) (Fig. 2G, N). Similarly, Papageorgiou et al. (1994) reported a gel containing 5% PG, 0.5% Ge, and 107.5 mM NaCl had Ge as the continuous phase.

3.3. Rheology

The rheological characterisation was performed for 6.67% (w/v) FG and FG-Ge mixtures (FGe2, FGe4, FGe5, FGe7, FGe9), with PG used as a reference. Ge at 2% (w/v) was also included for comparison, as 2% Ge was slightly above the maximum concentration (1.33%, w/v) of Ge in the FG-Ge mixed gel, and able to form a strong gel for rheological characterisation testing. Rheological properties of Ge at other concentrations (0.015–2%, w/v) are shown in Fig. S2 and Fig. S3. Cooling from 85 to 10 °C led to gelation, and the gel was melted during reverse heating (Fig. 3A–D). The T_g and T_m identified from the temperature sweep are shown in Table 2. The T_m and T_g of the pure components were in the order of FG < PG < Ge. The T_m increased significantly from FG at Ge:FG (w/w) ≥ 1:99. FGe4 (32.23 ± 0.15 °C) showed a similar T_m to that of PG (31.21 ± 0.01 °C). By contrast, an increase in T_g from FG was only found in FGe7 and FGe9. Moreover, the T_g of FGe7 and FGe9 were similar to that of Ge. This was caused by the formation of a Ge continuous gel in FGe7 and FGe9 (Lau, Tang, & Paulson, 2001), as the concentration of Ge (0.5–1.33%, w/v) was above the gelling concentration (≥0.167% w/v, Fig. S1). There were two steps of increased (decreased) G' and G'' during gelation (melting) of FGe7 and FGe9 (Fig. 3), in which the gelling and melting profile shifted towards that of Ge. When the solutions (gels) were cooled (heated), the increased (decrease) in G' and G'' at about 40 °C and 20 °C corresponded to the contribution from Ge and FG, respectively.

The gelling temperature is frequency dependent (Yang et al., 2018b); therefore, the Winter-Chambon equation was applied to determine critical gelling temperature (T_g*). From the multifrequency plots of tan δ *vs.* temperature (Fig. S4), the crossover point was determined as the critical T_g*. The T_g* of the samples was similar to the T_g from the temperature sweep. In a highly concentrated and fast gelation system, the method based on tan δ and Eq. (3) to determine n was more suitable than Eq. (2) (Michon, Cuvelier, & Launay, 1993; Pérez-Campos, Chavarría-Hernández, Tecante, Ramírez-Gilly, & Rodríguez-Hernández, 2012). The n value is shown in Fig. 4A. FG and PG (6.67%, w/v) showed a similar value of n (0.014–0.016), while Ge (2%, w/v) had a larger n at 0.038. The addition of Ge into FG increased n to about 0.056 in FGe7, followed by decreased to about 0.014 in FGe9. The low n value suggested that the system was highly elastic ($n = 1$ for pure elastic, $n = 0$ for pure viscous). The n value is not universal but dependent on gel history, the type of materials and their concentration (Michon et al., 1993). There were no previous reports of the n value for a Ge-FG gel.

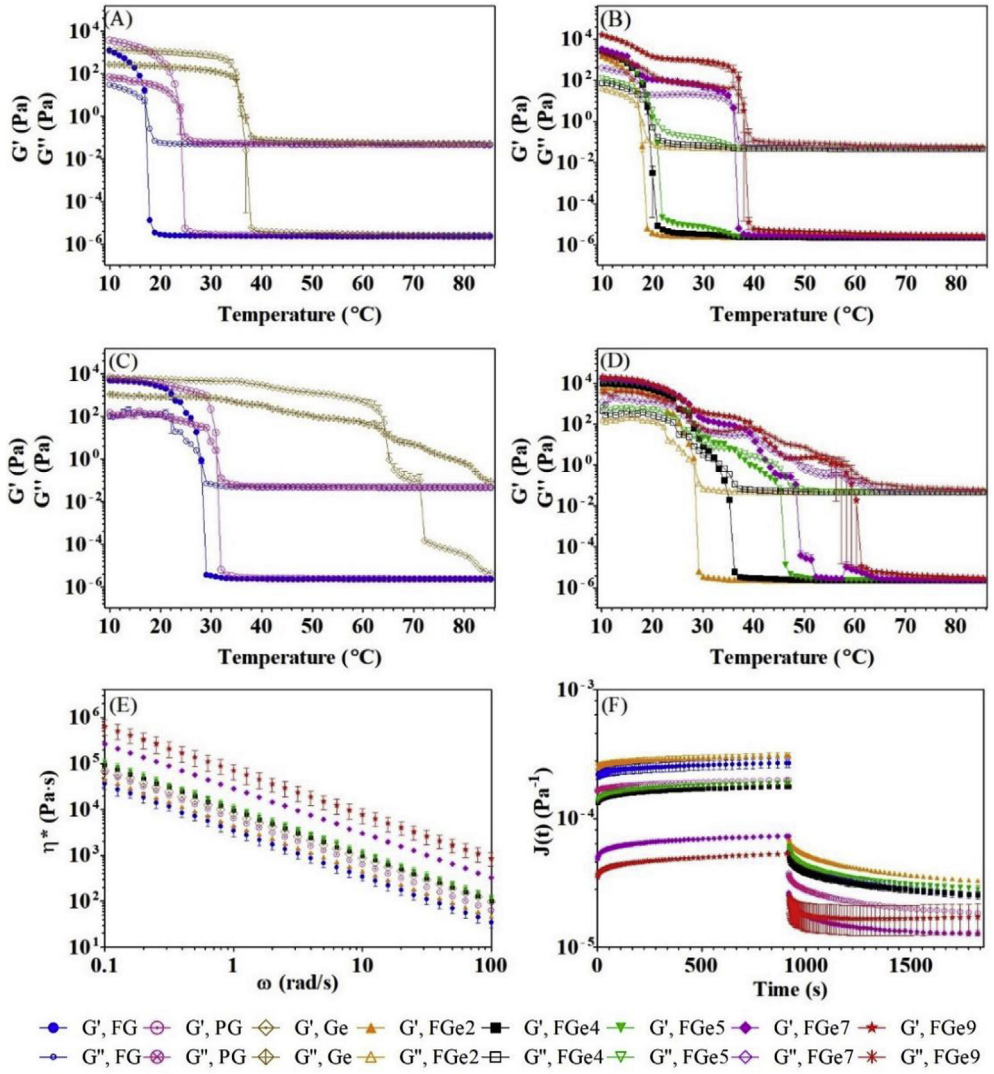

Fig. 3. Temperature sweep of (A, B) cooling and (C, D) heating cycle between 10 and 85 °C for (A, C) pure components (6.67%, w/v fish gelatin (FG), pork gelatin (PG) and 2%, w/v gellan (Ge)) as well as (B, D) FG-Ge mixtures (FGe2, FGe4, FGe5, FGe7, FGe9) and the characterisations of gel at 10 °C of (E) complex viscosity, η* as a function of angular frequency, ω; (F) creep-recovery compliance (J(t)) as a function of time.
*FGe2, FGe4, FGe5, FGe7, and FGe9 refer to FG-Ge mixtures with mixing ratios (Ge:FG, w/w) of 0.5:99.5, 1:99, 2.5:97.5, 7.5:92.5, and 20:80, respectively.

Michon et al. (1993) reported *n* values of 0.7 to 0.2 with increasing gelatin from 1.1 to 20.0% (w/w), while gellan (0.02–0.07%) with $CaCl_2$ (0.7–15 mM) had *n* values of 0.88–0.32 (Pérez-Campos et al., 2012). A low *n* value (< 0.2) was reported by Nordby, Kjøniksen, Nyström, and Roots (2003) in pectin-chitosan (1%).

At T_g*, the critical gel strength, S_g, was calculated using Eq. (5) and shown in Fig. 4B. Ge and FGe9 showed significantly greater S_g values than the rest of the samples ($P < 0.05$). S_g is related to the crosslinking density (Nordby et al., 2003). To further investigate the effect of Ge on FGe gels, S_g was normalised by [Ge] (%, w/v) (Fig. 4C). The addition of

Table 2
Summary of rheological test results of temperature sweep (reported as T_m and T_g), time sweep (modulus at 90 min, 10 °C) and frequency sweep (Eq. (6) parameters).

Sample	Temperature sweep		Time sweep		Frequency sweep	
	T_m (°C)	T_g (°C)	G′ (Pa)	G″ (Pa)	n_f	$K_f \times 10^3$ (Pa·s$^{(1-n_f)}$)
PG	31.21 ± 0.01^{d}	23.59 ± 0.37^{b}	6408 ± 312^{def}	15 ± 3^{e}	0.998 ± 0.003^{ab}	6.41 ± 0.42^{b}
FG	27.97 ± 0.15^{e}	16.94 ± 0.07^{c}	3461 ± 816^{f}	79 ± 16de	1.001 ± 0.000^{a}	3.53 ± 0.85^{b}
FGe2	28.08 ± 0.02^{e}	17.20 ± 0.05^{c}	4434 ± 358^{ef}	19 ± 3^{e}	0.996 ± 0.001^{ab}	4.55 ± 0.30^{b}
FGe4	32.23 ± 0.15^{d}	18.70 ± 0.23^{c}	9678 ± 393^{cd}	153 ± 10de	0.989 ± 0.001^{ab}	9.62 ± 0.32^{b}
FGe5	35.65 ± 0.27^{c}	19.26 ± 0.12^{bc}	10736 ± 1529^{c}	337 ± 211^{cd}	0.987 ± 0.002^{b}	10.83 ± 2.07^{b}
FGe7	39.20 ± 0.77^{b}	33.62 ± 2.38^{a}	28204 ± 1557^{b}	1817 ± 259^{b}	0.969 ± 0.001^{c}	28.62 ± 1.27^{b}
FGe9	39.82 ± 0.13^{b}	36.90 ± 1.03^{a}	57350 ± 4573^{a}	4936 ± 150^{a}	0.955 ± 0.006^{cd}	71.00 ± 2.58^{a}
Ge	62.97 ± 2.07^{a}	34.81 ± 0.66^{a}	7835 ± 1306^{cde}	533 ± 52^{c}	0.953 ± 0.006^{d}	7.99 ± 1.10^{b}

*Means with different lowercase letters within each column are significantly different ($P < 0.05$) among the different groups.
*FGe2, FGe4, FGe5, FGe7, and FGe9 refer to FG-Ge mixtures with mixing ratios (Ge:FG, w/w) of 0.5:99.5, 1:99, 2.5:97.5, 7.5:92.5, and 20:80, respectively.

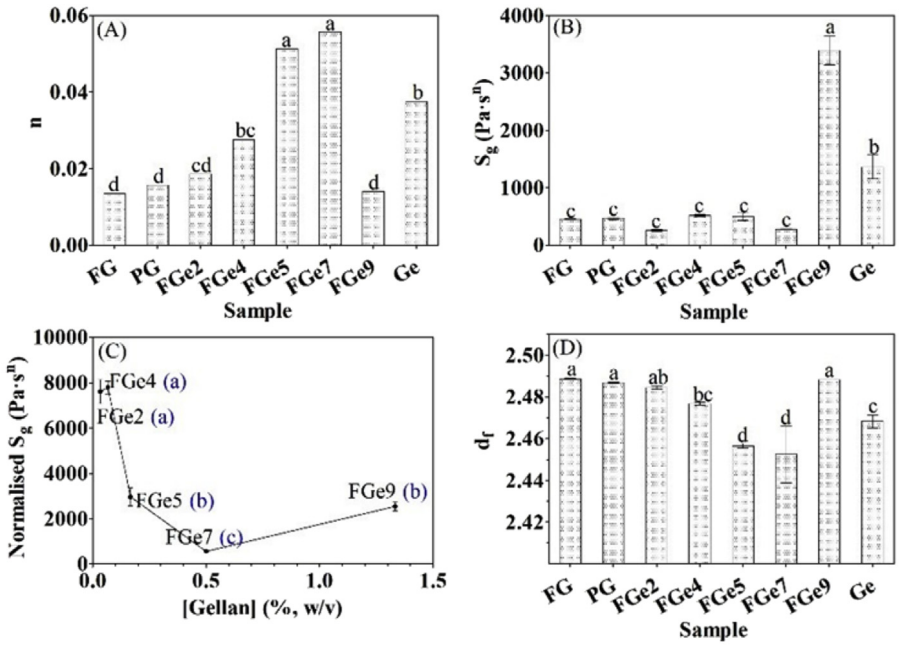

Fig. 4. Effect of gellan (GE) addition on the modification of (A) the critical relaxation modulus (n), (B) the critical gel strength (S_g) and (C) the normalised S_g, (D) the fractal dimension (d_f) of fish gelatin (FG).
*Means with different lowercase letters are significantly different ($P < 0.05$) among the different groups.
*Fig. 4(C), the data label is presented as "sample name (statistical label)".
*FGe2, FGe4, FGe5, FGe7, and FGe9 refer to FG-Ge mixtures with mixing ratios (Ge:FG, w/w) of 0.5:99.5, 1:99, 2.5:97.5, 7.5:92.5, and 20:80, respectively.

Table 3
Burgers model parameters of fish gelatin (FG), pork gelatin (PG), gellan (Ge), and the FG-Ge mixtures during creep phase (0–915.5 s).

Sample	$J_0 \times 10^{-5}$ (Pa^{-1})	$Jm_1 \times 10^{-5}$ (Pa^{-1})	$Jm_2 \times 10^{-5}$ (Pa^{-1})	$Jm_3 \times 10^{-5}$ (Pa^{-1})	λ_1 (s)	λ_2 (s)	λ_3 (s)	$\eta_0 \times 10^{10}$ (Pa·s)	R^2
PG	16.3 ± 0.9^{b}	1.47 ± 0.10^{cd}	0.44 ± 0.02^{c}	0.24 ± 0.02^{c}	208 ± 18^{ab}	24.1 ± 7.1^{ab}	2.32 ± 1.02^{a}	6.34 ± 0.41^{b}	0.99993
FG	21.9 ± 3.1^{a}	2.07 ± 0.40^{ab}	0.69 ± 0.13^{b}	0.40 ± 0.16^{bc}	246 ± 9^{a}	32.2 ± 0.9^{a}	3.14 ± 0.39^{a}	4.41 ± 0.04^{bc}	0.99992
FGe2	24.8 ± 1.9^{a}	2.51 ± 0.04^{a}	0.84 ± 0.05^{ab}	0.68 ± 0.11^{a}	203 ± 18^{ab}	28.9 ± 9.1^{ab}	3.28 ± 0.58^{a}	3.84 ± 0.15^{c}	0.99997
FGe4	13.1 ± 0.0^{b}	1.91 ± 0.30^{bc}	0.76 ± 0.08^{b}	0.52 ± 0.11^{ab}	175 ± 21^{ab}	23.1 ± 4.2^{ab}	2.03 ± 0.41^{a}	5.56 ± 0.05^{bc}	0.99999
FGe5	13.5 ± 0.5^{b}	2.26 ± 0.05^{ab}	0.93 ± 0.03^{a}	0.71 ± 0.02^{a}	177 ± 12^{ab}	22.4 ± 1.9^{ab}	2.29 ± 0.05^{a}	6.16 ± 0.40^{b}	0.99997
FGe7	4.77 ± 0.1^{c}	1.01 ± 0.08^{de}	0.44 ± 0.02^{c}	0.38 ± 0.03^{bc}	177 ± 15^{ab}	24.8 ± 6.0^{ab}	2.62 ± 0.42^{a}	12.25 ± 0.64^{a}	0.99995
FGe9	3.41 ± 0.1^{c}	0.68 ± 0.06^{e}	0.26 ± 0.05^{d}	0.27 ± 0.09^{c}	157 ± 85^{b}	16.5 ± 11.6^{b}	1.92 ± 0.15^{a}	12.70 ± 2.83^{a}	0.99993

*Means with different lowercase letters within each column are significantly different ($P < 0.05$) among different groups.
*FGe2, FGe4, FGe5, FGe7, and FGe9 refer to FG-Ge mixtures with mixing ratios (Ge:FG, w/w) of 0.5:99.5, 1:99, 2.5:97.5, 7.5:92.5, and 20:80, respectively.

Ge decreased S_g above FGe4 to a minimum in FGe7, and then increased slightly in FGe9. The size of the complex coacervates increased with increasing [Ge] up to FGe7, thereby increasing the distance between the junction zones, resulted in a decrease in normalised S_g. Decreases in S_g were reported when graphene oxide was filled into a κ-carrageenan network (Liu, Bao, & Li, 2016), and when pectin was added into chitosan (Nordby et al., 2003). The normalised S_g value of FGe9 was lower than that of FGe2 and FGe4, suggesting that the larger value of S_g (Fig. 4B) was caused by the high concentration of Ge and subsequent Ge continuous gel formation, which increased the overall gel density and strength (Liu, Chan, & Li, 2015).

The density of the network could also be determined based on fractal dimension, d_f, which is related to n through the following equation (Muthukumar, 1989),

$$n = \frac{d(\, d+ 2 - 2d_f)}{2(\, d+ 2 - d_f)}. \quad (11)$$

where d is the space dimension (d = 3).

From Eq. (11) and Fig. 4D, d_f was between 2.45 and 2.50, which was similar to the report of Nordby et al. (2003) in the pectin/chitosan system. The increase in Ge:FG (w/w) up to 7.5:92.5, showed a decreased d_f, caused by the large complex coacervates formed which led to a loose network. In FGe9, d_f increased to the level of FG, as the large complex coacervates disappeared in FGe9. The network density (d_f) and strength (S_g) of FGe9 increased because of the FG-Ge bi-continuous network formation.

The gel was formed and matured at 10 °C (Fig. S5), the G′ and G″ at 90 min of storage were compared in Table 2. The G′ of all samples was greater than the G″, indicated a strong gel system (Mohtar et al., 2013). The G′ and G″ of FGe gels (except the G″ of FGe2) increased with increasing Ge:FG (w/w), and even greater than the sum of FG and Ge in FGe7 and FGe9. No significant differences ($P < 0.05$) in G′ and G″ was found between FGe4 and PG. The frequency sweep at 10 °C suggested that the G′ and G″ were almost independent of ω (Fig. S5). The η* value, however, showed a power law dependent on ω (Fig. 3E). The parameters of Eq. (6) are shown in Table 2. The low n_f value indicated that the system was close to an elastic solid ($n_f = 1$ for elastic solid, $n_f = 0$ for a viscous fluid) (Nakauma et al., 2016). The Ge continuous gel formation resulted in n_f values of FGe7, FGe9, and Ge that were significantly lower ($P < 0.05$) than those of PG, FG, FGe2, FGe4, and FGe5. K_f increased significantly in FGe9 compared with rest of the samples.

The gels were subjected to a creep-recovery test (Fig. 3F), and Burgers model was applied (Table 3 & Table 4) with $R^2 > 0.999$. Ge at 2% (w/v) cannot withstand the shear stress of 200 Pa, as Ge was reported to be a yield stress fluid (García, Alfaro, & Muñoz, 2015). The low value of J_0 and J_{max} indicated the formation of a hard and firm sample (Fu, Che, Li, Wang, & Adhikari, 2016; Yilmaz, Karamam, Dogan, Yetim, & Kayacier, 2012). Increases in J_0 and J_{max} were found in FGe2 compared with that in FG, and subsequently decreased to a minimum in FGe9. The J_m value followed a similar trend to J_0 and J_{max}. The λ value indicated no significant difference among the samples ($P > 0.05$). The resistance to flow, indicated by η_0 (Fu et al., 2016), increased significantly in FGe7 and FGe9 compared with that in FG. The percentage

Table 4
Burgers model parameters of fish gelatin (FG), pork gelatin (PG), gellan (Ge), and the FG-Ge mixtures during the recovery phase (915.5–1820 s).

Sample	$J_{max} \times 10^{-5}$ (Pa^{-1})	$J_0 \times 10^{-5}$ (Pa^{-1})	$Jm_1 \times 10^{-5}$ (Pa^{-1})	$Jm_2 \times 10^{-5}$ (Pa^{-1})	$Jm_3 \times 10^{-5}$ (Pa^{-1})	λ_1 (s)	λ_2 (s)	λ_3 (s)	Je (%)	Jv (%)	R^2
PG	19.9 ± 1.0^{b}	16.2 ± 0.9^{b}	1.02 ± 0.18^{c}	0.44 ± 0.01^{c}	0.22 ± 0.10^{d}	220 ± 19^{a}	30.4 ± 20.1^{a}	4.11 ± 0.26^{a}	89.5 ± 1.2^{a}	10.5 ± 1.2^{b}	0.99967
FG	27.1 ± 3.8^{a}	21.4 ± 3.0^{a}	1.54 ± 0.23^{ab}	0.58 ± 0.09^{bc}	0.44 ± 0.07^{abc}	208 ± 51^{a}	30.6 ± 5.1^{a}	2.88 ± 0.15^{ab}	88.4 ± 0.4^{a}	11.6 ± 0.4^{b}	0.99983
FGe2	31.2 ± 1.9^{a}	23.9 ± 1.8^{a}	1.84 ± 0.18^{a}	0.83 ± 0.10^{a}	0.60 ± 0.04^{a}	224 ± 32^{a}	34.2 ± 3.6^{a}	3.55 ± 0.37^{ab}	87.3 ± 1.6^{a}	12.7 ± 1.6^{b}	0.99995
FGe4	17.9 ± 0.4^{b}	12.5 ± 0.1^{b}	1.22 ± 0.03^{bc}	0.65 ± 0.08^{b}	0.51 ± 0.07^{ab}	202 ± 0^{a}	29.3 ± 5.9^{a}	2.96 ± 0.73^{ab}	83.1 ± 1.3^{a}	16.9 ± 1.3^{b}	0.99986
FGe5	18.9 ± 0.5^{b}	12.6 ± 0.5^{b}	1.50 ± 0.05^{b}	0.73 ± 0.04^{ab}	0.62 ± 0.00^{a}	185 ± 5^{a}	26.6 ± 0.8^{a}	2.98 ± 0.66^{ab}	82.0 ± 0.9^{a}	18.0 ± 0.9^{b}	0.99993
FGe7	7.3 ± 0.1^{c}	4.6 ± 0.1^{c}	0.59 ± 0.03^{d}	0.45 ± 0.06^{c}	0.38 ± 0.03^{ab}	237 ± 32^{a}	41.2 ± 9.0^{a}	3.93 ± 0.77^{a}	82.5 ± 0.2^{a}	17.5 ± 0.2^{b}	0.99975
FGe9	5.3 ± 0.2^{c}	3.0 ± 0.7^{c}	0.27 ± 0.02^{e}	0.28 ± 0.06^{d}	0.27 ± 0.13^{bcd}	220 ± 19^{a}	27.3 ± 0.8^{a}	2.28 ± 0.91^{b}	70.6 ± 12.4^{b}	19.4 ± 12.4^{a}	0.99923

*Means with different lowercase letters within each column are significantly different ($P < 0.05$) among the different groups.
*FGe2, FGe4, FGe5, FGe7, and FGe9 refer to FG-Ge mixtures with mixing ratios (Ge:FG, w/w) of 0.5:99.5, 1:99, 2.5:97.5, 7.5:92.5, and 20:80, respectively.

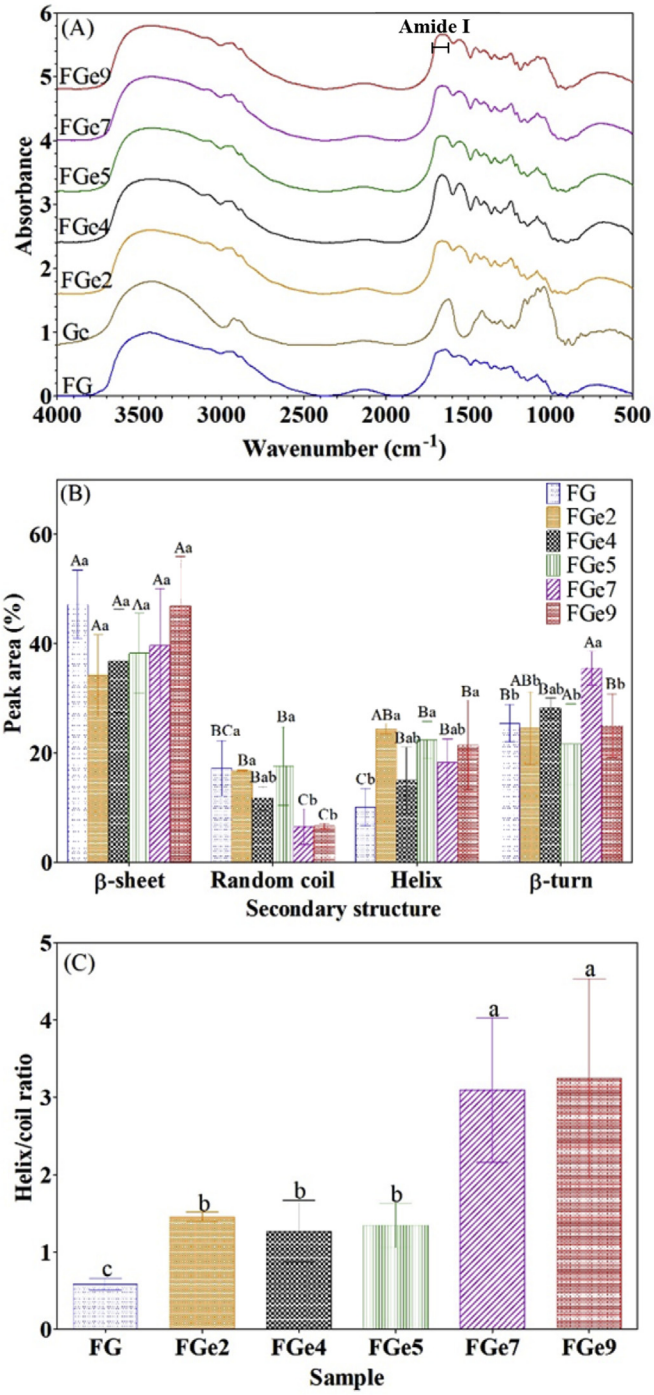

Fig. 5. (A) Fourier transform infrared (FTIR) spectra of fish gelatin (FG), gellan (Ge), and FG-Ge mixtures (FGe); amide I was deconvoluted and curve-fitted ($R^2 > 0.99$), the results are presented as (B) the secondary structure distribution and the (C) helix/coil ratio.
*Means with different lowercase (uppercase) letters are significantly different ($P < 0.05$) among the different samples (within the same sample).
*FGe2, FGe4, FGe5, FGe7, and FGe9 refer to FG-Ge mixtures with mixing ratios (Ge:FG, w/w) of 0.5:99.5, 1:99, 2.5:97.5, 7.5:92.5, and 20:80, respectively.

of elastic compliance, J_e (%), was calculated from the following equation,

$$J_e\,(\%) = \frac{J_{0_r} + J_{m_r}}{J_{max}} \times 100\% \tag{12}$$

and the percentage of the viscous compliance,

Table 5
FTIR peak table of fish gelatin (FG), gellan (Ge), and FG-Ge mixed gels (FGe2, FGe4, FGe5, FGe7, FGe9).

Region	Wavenumber (cm^{-1})							Description
	FG	Ge	FGe2	FGe4	FGe5	FGe7	FGe9	
Amide A	3434.8 ± 0.9^{a}	3434.3 ± 0.3^{a}	3433.5 ± 2.5^{a}	3435.9 ± 0.5^{a}	3435.0 ± 0.6^{a}	3434.7 ± 1.0^{a}	3430.2 ± 10.8^{a}	OH stretch (Ge), NH stretch
Amide B	3085.7 ± 2.9^{a}		3087.5 ± 1.9^{a}	3083.2 ± 0.6^{a}	3087.2 ± 1.6^{a}	3088.3 ± 1.9^{a}	3090.3 ± 4.9^{a}	NH bend
	2935.7 ± 3.8^{b}	2924.6 ± 0.5^{c}	2960.6 ± 1.3^{a}	2958.8 ± 0.0^{a}	2960.0 ± 0.7^{a}	2939.8 ± 2.5^{b}	2937.1 ± 1.9^{b}	CH_2 stretch
	2880.0 ± 0.7^{b}	2893.8 ± 3.3^{a}	2881.4 ± 0.3^{b}	2880.7 ± 0.1^{b}	2881.0 ± 0.4^{b}	2883.0 ± 4.7^{b}	2882.6 ± 0.4^{b}	CH_3 stretch
Amide I	1637.2 ± 1.0^{c}	1619.6 ± 2.1^{d}	1660.2 ± 3.3^{ab}	1660.5 ± 1.7^{ab}	1664.2 ± 2.3^{a}	1658.3 ± 0.4^{b}	1657.3 ± 3.2^{b}	C=O stretch, COO^- coupled with H-bond, glycosidic link (Ge)
Amide II	1557.7 ± 3.3^{a}		1550.8 ± 2.7^{b}	1551.9 ± 1.3^{b}	1551.2 ± 0.5^{b}	1552.8 ± 1.0^{b}	1553.4 ± 1.5^{b}	CN stretch, NH bend
	1454.4 ± 1.3^{a}		1453.5 ± 0.9^{a}	1452.1 ± 0.5^{a}	1454.2 ± 2.2^{a}	1453.9 ± 1.7^{a}	1453.3 ± 0.3^{a}	CH_2 bend
	1402.0 ± 1.8^{c}	1415.9 ± 0.7^{a}	1403.9 ± 0.8^{bc}	1403.8 ± 0.1^{bc}	1403.8 ± 1.2^{bc}	1403.0 ± 1.6^{c}	1405.4 ± 0.8^{b}	CH bend (Ge), COO− stretch
	1339.5 ± 1.1^{ab}	1340.3 ± 0.2^{a}	1338.5 ± 0.2^{ab}	1338.0 ± 1.5^{ab}	1337.7 ± 0.4^{b}	1339.2 ± 1.5^{ab}	1339.5 ± 0.3^{ab}	CH_2 wag
	1282.7 ± 2.6^{b}	1301.0 ± 0.3^{a}	1281.6 ± 0.5^{b}	1281.5 ± 0.1^{b}	1282.6 ± 1.9^{b}	1281.9 ± 0.2^{b}	1283.4 ± 0.4^{b}	C−O stretch (Ge)
Amide III	1248.4 ± 11.7^{a}	1236.8 ± 0.2^{b}	1239.7 ± 0.4^{ab}	1240.2 ± 0.2^{ab}	1241.2 ± 0.1^{ab}	1241.1 ± 1.2^{ab}	1240.7 ± 0.7^{ab}	NH deformation, CN stretch.
Fingerprint	1162.5 ± 0.8^{a}	1155.3 ± 0.5^{c} 1107.1 ± 0.6	1162.3 ± 0.3^{a}	1161.1 ± 0.1^{ab}	1161.4 ± 0.7^{ab}	1160.2 ± 0.7^{b}	1154.3 ± 0.6^{c}	C−O stretch, skeletal stretch
	1082.8 ± 0.4^{a}	1077.0 ± 0.3^{d}	1082.1 ± 0.6^{ab}	1081.6 ± 0.0^{b}	1081.4 ± 0.3^{b}	1081.3 ± 0.4^{b}	1079.2 ± 0.6^{c}	
	1032.6 ± 0.1^{d}	1038.3 ± 0.4^{b}	1032.9 ± 0.4^{cd}	1032.8 ± 0.1^{cd}	1032.9 ± 0.3^{cd}	1033.6 ± 0.4^{c}	1046.9 ± 0.6^{a}	
	973.4 ± 0.2^{c}	993.4 ± 0.2^{a}	974.5 ± 0.7^{bc}	974.6 ± 0.1^{bc}	974.8 ± 0.4^{bc}	975.6 ± 1.1^{b}		
	937.5 ± 1.2^{c}	945.6 ± 0.5^{a}	937.6 ± 1.1^{c}	938.6 ± 0.7^{c}	938.9 ± 0.3^{c}	938.6 ± 0.3^{c}	940.3 ± 0.2^{b}	
	923.0 ± 1.0^{ab}	923.8 ± 0.2^{a}	922.2 ± 0.5^{ab}	920.9 ± 0.9^{b}	921.8 ± 0.2^{ab}	923.8 ± 2.0^{a}	922.8 ± 0.4 ^{ab}	
	872.4 ± 1.3^{c}	891.1 ± 0.1^{a} 837.1 ± 0.5	872.6 ± 1.7^{c}	874.7 ± 0.6^{bc}	872.4 ± 1.2^{c}	872.7 ± 1.7^{c}	876.7 ± 2.4^{b}	

*Means with different lowercase letters within each column are significantly different ($P < 0.05$) among different groups.
*Description of the peaks was according to the reports of Noor et al. (2012); Sow and Yang (2015); Sudhamani et al. (2003).
*FGe2, FGe4, FGe5, FGe7, and FGe9 refer to FG-Ge mixtures with mixing ratios (Ge:FG, w/w) of 0.5:99.5, 1:99, 2.5:97.5, 7.5:92.5, and 20:80, respectively.

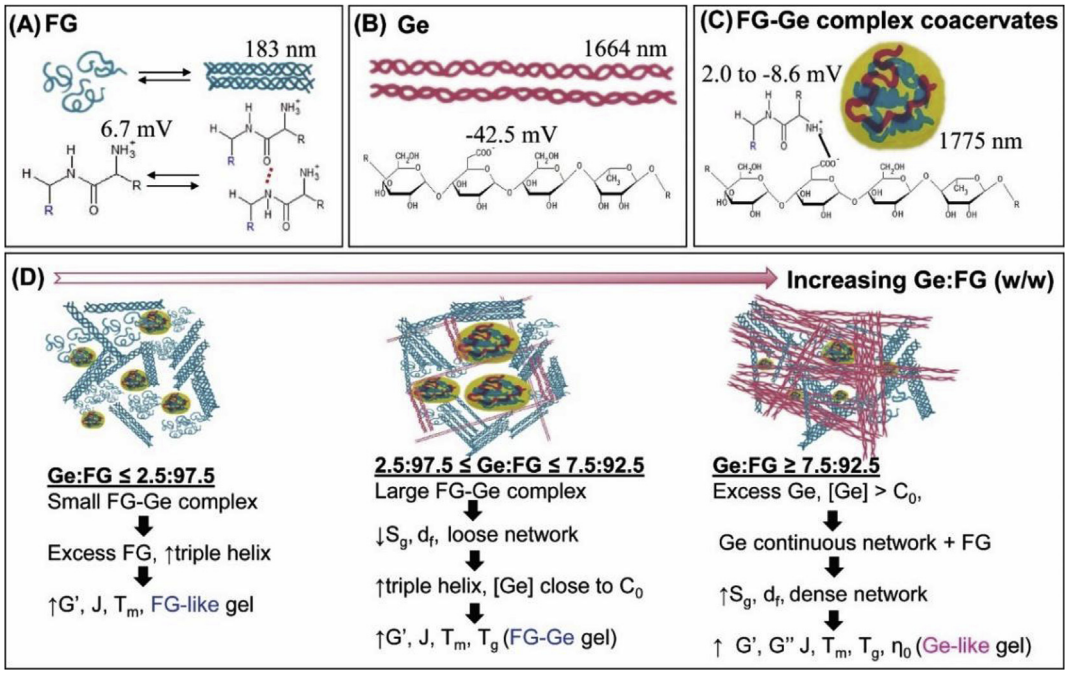

Fig. 6. Schematic diagram illustrating (A) fish gelatin (FG), (B) gellan (Ge), (C) the FG-Ge complex coacervates formed by electrostatic interaction and (D) the progressive modification of FG with increasing Ge:FG (w/v) on the structure and rheological properties.
*C_0 indicates the gelling concentration of Ge shown in Fig. S1.

$$J_y(\%) = 100\% - J_e(\%). \quad (13)$$

FGe9 showed significantly lower J_e (%) and higher J_v (%) than rest of the samples, which could be attributed to the formation of a bi-continuous gel with Ge as the continuous phase. At the same ratio of KC to FG as in FGe9, a bi-continuous gel with low compliance value has been reported (Sow et al., 2018a). Overall, FGe4 showed a close match for the parameters J_0, J_{max}, J_{m1}, η_0, J_e (%) and J_v (%) with those of PG. The FG-Ge gel was a more efficient potential replacer of PG with lower polysaccharide:FG (w/w) of 1:99 compared with 4:96 in the FG-KC gel (Sow et al., 2018a).

3.4. FTIR

The FTIR spectra and the positions of the absorption peaks are shown in Fig. 5A and Table 5. There was significant peak shifting of FG at 2936, 1637, 1558, 1162, 1082, 1032, 973, 937, and 872 cm^{-1} compared with the FGe samples. The shifting in the fingerprint region (1162 cm^{-1} and below) was largely caused by the contribution of Ge C−O and skeletal stretch from primary or secondary alcohol

(Sudhamani, Prasad, & Udaya Sankar, 2003), which was more pronounced at a larger ratio of Ge:FG (w/w). Amide I peak is useful in analysis of protein secondary structure, the position of amide I was affected by hydrogen bonding and protein conformation (Sinthusamran et al., 2014). The amide I peak was shifted to 1657–1664 cm^{-1} in FGe samples, indicating more helix structure had formed (Sow & Yang, 2015). Meanwhile, the peak of amide II showed a low shifting of wavenumber to 1553–1550 cm^{-1}, which might be caused by hydrogen bond formation to the CN or NH functional group (Sow et al., 2017).

The amide I peak was deconvoluted and peak fitted ($R^2 > 0.99$). The component peaks were assigned to various secondary structures based on their position (Sow et al., 2017), the peak area (%) is shown in Fig. 5B. The helix to coil ratio can be used as an estimation of triple helix content (Sow et al., 2017), is shown in Fig. 5C. There were increases in the helix/coil ratio with Ge addition into FG, in the order of FG < FGe2, FGe4, FGe5 < FGe7, FGe9.

3.5. Schematic model

Based on the results of sections *3.1* to *3.4*, a schematic model was proposed to explain the modification of FG by Ge addition. Above the pI, FG was positively charged (6.7 mV) because of the NH_3^+ functional group of the amino acids. When the temperature reduced, FG underwent coil to triple-helix formation with the aid of intermolecular hydrogen bonds to initiate gelation (Fig. 6A). While for Ge, the COO^- provided an overall anionic charged (−42.5 mV) of the molecules, and a double helix was formed during molecular ordering of Ge (Fig. 6B). The positively charged FG and negatively charged Ge could associate to form complex coacervates via electrostatic interaction (Fig. 6C). Upon mixing of Ge and FG (Fig. 6D), at a low ratio of Ge:FG (w/w) ≤ 2.5:97.5 (FGe5), the increment in the strength of the gel (*G′*, J) was caused by the increased triple helix content. Excess FG that did not interact with Ge to form complex coacervates could be restrained using a lower amount of solvent, and increasing the effective concentration of FG, thereby increased the intermolecular association of FG into the triple helix. The physical properties of the gel were similar to those of FG when the continuous phase was FG. Increasing the Ge:FG ratio to ≤7.5:92.5 formed large complex coacervates, which led to an opaque and loose network structure (low S_g, d_f). When the Ge concentration was close to gelling concentration ($C_0 \geq 0.167\%$, w/v, Fig. S1), the network strength was supported by both FG and Ge, in which FG was the continuous phase (T_g similar to FG) in FGe5 and Ge was the continuous phase in FGe7 (T_g similar to Ge). A complete phase inversion occurred at a high ratio of Ge:FG (w/w) ≥ 7.5:92.5. In the FGe9, complex coacervates almost completely disappeared or decreased in size, and a Ge continuous gel network was formed followed by an FG gel network. Therefore, the density of the network increased significantly (high S_g, d_f), the gel showed characteristics of Ge (low n_f, J_e(%), high T_g, T_m, η_0, and J_v(%)).

3.6. Conclusion

Gellan modified the structure and physical properties of FG, depending on the mixing ratio. Maximum coacervate size and turbidity were observed at a Ge:FG (w/w) of 7.5:92.5, accompanied by phase inversion of the FG continuous phase into the Ge continuous phase when Ge:FG (w/w) ≥ 7.5:92.5. At lower mixing ratios, the FG-Ge gel benefited from the excluded volume effect; where an increase in the effective FG concentration (caused by the repulsion effect of FG-Ge coacervates) and the amount of triple helix improved the strength and thermal stability of the gel, without drastic changes in appearance and physical properties of gelatin. Gels at 1:99 of Ge:FG (w/w) ratio matched the physical properties of PG, which suggested that this ratio could be an efficient replacement for PG. The Winter-Chambon law was successfully applied to the FG-Ge system, with the *n* value being reported for the first time in such a system.

Acknowledgements

This work was funded by the Singapore Ministry of Education Academic Research Fund Tier 1 (R-143-000-A40-114), projects 31371851 and 31471605 supported by NSFC, and a project funded by Fujian Putian Sea-100 Food Co., Ltd. (R-143-000-633-597).

Appendix A. Supplementary data

Supplementary data to this article can be found online at https://doi.org/10.1016/j.foodhyd.2018.12.006.

Abbreviation

BG	beef gelatin
CLSM	Confocal laser scanning microscope
FG	fish gelatin
FTIR	Fourier transform infrared spectroscopy
Ge	low acyl gellan
KC	κ-carrageenan
PG	pork gelatin
T_g	gelling temperature
T_m	melting temperature

References

Banerjee, S., & Bhattacharya, S. (2011). Compressive textural attributes, opacity and syneresis of gels prepared from gellan, agar and their mixtures. *Journal of Food Engineering, 102*, 287–292.

Chilvers, G. R., & Morris, V. J. (1987). Coacervation of gelatin-gellan gum mixtures and their use in microencapsulation. *Carbohydrate Polymers, 7*, 111–120.

Desilver, D., & Masci, D. (2017). World's Muslim population more widespread than you might think. *Fact Tank*. Retrieved 10-06-2018 from Pew Research Center: http://pewrsr.ch/116QRmk.

Feng, X., Bansal, N., & Yang, H. (2016). Fish gelatin combined with chitosan coating inhibits myofibril degradation of golden pomfret (*Trachinotus blochii*) fillet during cold storage. *Food Chemistry, 200*, 283–292.

Feng, X., Fu, C., & Yang, H. (2017). Gelatin addition improves nutrient retention, texture and mass transfer of fish balls without altering their nanostructure during boiling. *LWT-Food Science and Technology, 77*, 142–151.

Feng, X., Hang, S., Zhou, Y., Liu, Q., & Yang, H. (2018). Bromelain kinetics and mechanism on myofibril from golden pomfret (*Trachinotus blochii*). *Journal of Food Science, 83*, 2148–2158.

Feng, X., Ng, V. K., Mikš-Krajnik, M., & Yang, H. (2017). Effects of fish gelatin and tea polyphenol coating on the spoilage and degradation of myofibril in fish fillet during cold storage. *Food and Bioprocess Technology, 10*, 89–102.

Fu, Z., Che, L., Li, D., Wang, L., & Adhikari, B. (2016). Effect of partially gelatinized corn starch on the rheological properties of wheat dough. *LWT - Food Science and Technology, 66*, 324–331.

García, M. C., Alfaro, M. C., & Muñoz, J. (2015). Yield stress and onset of nonlinear time-dependent rheological behaviour of gellan fluid gels. *Journal of Food Engineering, 159*, 42–47.

Haug, I. J., Draget, K. I., & Smidsrød, O. (2004). Physical and rheological properties of fish gelatin compared to mammalian gelatin. *Food Hydrocolloids, 18*, 203–213.

Hu, B., Lu, Y., Zhao, Q., & Matsukawa, S. (2017). A study on the gelation behavior of solutions of native gellan, deacylated gellan, and their mixture by water ^1H T_2 measurements. *Food Hydrocolloids, 72*, 47–51.

Ikeda, S., & Henry, K. (2016). Effects of partial replacement of gelatin in high sugar gels with gellan on their textural, rheological, and thermal properties. *Food Biophysics, 11*, 400–409.

Lau, M. H., Tang, J., & Paulson, A. T. (2000). Texture profile and turbidity of gellan/gelatin mixed gels. *Food Research International, 33*, 665–671.

Lau, M. H., Tang, J., & Paulson, A. T. (2001). Effect of polymer ratio and calcium concentration on gelation properties of gellan/gelatin mixed gels. *Food Research International, 34*, 879–886.

Lee, K. Y., Shim, J., Bae, I. Y., Cha, J., Park, C. S., & Lee, H. G. (2003). Characterization of gellan/gelatin mixed solutions and gels. *LWT - Food Science and Technology, 36*, 795–802.

Lee, K. Y., Shim, J., & Lee, H. G. (2004). Mechanical properties of gellan and gelatin composite films. *Carbohydrate Polymers, 56*, 251–254.

Liu, S., Bao, H., & Li, L. (2016). Thermoreversible gelation and scaling laws for graphene oxide-filled κ-carrageenan hydrogels. *European Polymer Journal, 79*, 150–162.

Liu, S., Chan, W. L., & Li, L. (2015). Rheological properties and scaling laws of κ-carrageenan in aqueous solution. *Macromolecules, 48*, 7649–7657.

Michon, C., Cuvelier, G., & Launay, B. (1993). Concentration dependence of the critical viscoelastic properties of gelatin at the gel point. *Rheologica Acta, 32*, 94–103.

Mohtar, N. F., Perera, C. O., Quek, S.-Y., & Hemar, Y. (2013). Optimization of gelatine gel preparation from New Zealand hoki (*Macruronus novaezelandiae*) skins and the effect

of transglutaminase enzyme on the gel properties. *Food Hydrocolloids, 31*, 204–209.
Morris, E. R., Nishinari, K., & Rinaudo, M. (2012). Gelation of gellan – a review. *Food Hydrocolloids, 28*, 373–411.
Muthukumar, M. (1989). Screening effect on viscoelasticity near the gel point. *Macromolecules, 22*, 4656–4658.
Nakauma, M., Funami, T., Fang, Y., Nishinari, K., Draget, K. I., & Phillips, G. O. (2016). Calcium binding and calcium-induced gelation of sodium alginate modified by low molecular-weight polyuronate. *Food Hydrocolloids, 55*, 65–76.
Noor, I. S. M., Majid, S. R., Arof, A. K., Djurado, D., Claro Neto, S., & Pawlicka, A. (2012). Characteristics of gellan gum–$LiCF_3SO_3$ polymer electrolytes. *Solid State Ionics, 225*, 649–653.
Nordby, M. H., Kjøniksen, A.-L., Nyström, B., & Roots, J. (2003). Thermoreversible gelation of aqueous mixtures of pectin and chitosan. Rheology. *Biomacromolecules, 4*, 337–343.
Pang, Z., Deeth, H., Yang, H., Prakash, S., & Bansal, N. (2017). Evaluation of tilapia skin gelatin as a mammalian gelatin replacer in acid milk gels and low-fat stirred yogurt. *Journal of Dairy Science, 100*, 3436–3447.
Papageorgiou, M., Kasapis, S., & Richardson, R. K. (1994). Steric exclusion phenomena in gellan/gelatin systems I. Physical properties of single and binary gels. *Food Hydrocolloids, 8*, 97–112.
Pérez-Campos, S. J., Chavarría-Hernández, N., Tecante, A., Ramírez-Gilly, M., & Rodríguez-Hernández, A. I. (2012). Gelation and microstructure of dilute gellan solutions with calcium ions. *Food Hydrocolloids, 28*, 291–300.
Petcharat, T., & Benjakul, S. (2017). Property of fish gelatin gel as affected by the incorporation of gellan and calcium chloride. *Food Biophysics, 12*, 339–347.
Pranoto, Y., Lee, C. M., & Park, H. J. (2007). Characterizations of fish gelatin films added with gellan and κ-carrageenan. *LWT - Food Science and Technology, 40*, 766–774.
Sinthusamran, S., Benjakul, S., & Kishimura, H. (2014). Characteristics and gel properties of gelatin from skin of seabass (*Lates calcarifer)* as influenced by extraction conditions. *Food Chemistry, 152*, 276–284.
Sow, L. C., Chong, J. M. N., Liao, Q. X., & Yang, H. (2018a). Effects of κ-carrageenan on the structure and rheological properties of fish gelatin. *Journal of Food Engineering, 239*, 92–103.
Sow, L. C., Kong, K., & Yang, H. (2018b). Structural modification of fish gelatin by the addition of gellan, κ-carrageenan, and salts mimics the critical physicochemical properties of pork gelatin. *Journal of Food Science, 83*, 1280–1291.
Sow, L. C., Peh, Y. R., Pekerti, B. N., Fu, C., Bansal, N., & Yang, H. (2017). Nanostructural analysis and textural modification of tilapia fish gelatin affected by gellan and calcium chloride addition. *LWT - Food Science and Technology, 85*, 137–145.
Sow, L. C., & Yang, H. (2015). Effects of salt and sugar addition on the physicochemical properties and nanostructure of fish gelatin. *Food Hydrocolloids, 45*, 72–82.
Sudhamani, S. R., Prasad, M. S., & Udaya Sankar, K. (2003). DSC and FTIR studies on gellan and polyvinyl alcohol (PVA) blend films. *Food Hydrocolloids, 17*, 245–250.
Wang, Y., & Padua, G. W. (2010). Formation of zein microphases in ethanol-water. *Langmuir, 26*, 12897–12901.
Winter, H. H., & Chambon, F. (1986). Analysis of linear viscoelasticity of a crosslinking polymer at the gel point. *Journal of Rheology, 30*, 367–382.
Yang, Z., Yang, H., & Yang, H. (2018a). Characterisation of rheology and microstructures of κ-carrageenan in ethanol-water mixtures. *Food Research International, 107*, 738–746.
Yang, Z., Yang, H., & Yang, H. (2018b). Effects of sucrose addition on the rheology and microstructure of κ-carrageenan gel. *Food Hydrocolloids, 75*, 164–173.
Yilmaz, M. T., Karaman, S., Dogan, M., Yetim, H., & Kayacier, A. (2012). Characterization of O/W model system meat emulsions using shear creep and creep recovery tests based on mechanical simulation models and their correlation with texture profile analysis (TPA) parameters. *Journal of Food Engineering, 108*, 327–336.
Zhou, P., Mulvaney, S. J., & Regenstein, J. M. (2006). Properties of Alaska pollock skin gelatin: A comparison with tilapia and pork skin gelatins. *Journal of Food Science, 71*, C313–C321.